Hindawi Publishing Corporation
Journal of Nanomaterials
Volume 2015, Article ID 269019, 8 pages
http://dx.doi.org/10.1155/2015/269019

Research Article

Preparation of Mixed Semiconductors for Methyl Orange Degradation

Sangeeta Adhikari and Debasish Sarkar

Department of Ceramic Engineering, National Institute of Technology, Rourkela, Odisha 769008, India

Correspondence should be addressed to Debasish Sarkar; dsarkar@nitrkl.ac.in

Received 4 April 2015; Accepted 17 May 2015

Academic Editor: Anh-Tuan Le

Attempts were made to compare the photocatalytic efficacy in between quasi-fiber and near spherical commercial grade ZnO through the addition of monoclinic WO_3 nanocuboid. Mixed oxide semiconductors were assessed for their dye degradation performance under irradiation of visible light energy. Surface area and the particle morphology pattern have an influence on the resultant photocatalytic features of these mixed oxide composites. The high porous quasi-fibrous ZnO was successfully fabricated by a simple solution combustion method. It is deliberately made of clusters of primary near spherical particles that supports WO_3 nanocuboid embedment and shows interactive characteristics in comparison to the counterpart commercial near spherical ZnO combined with WO_3. The photocatalytic activity significantly increases up to 95% under visible radiation for 90 min due to high surface area imparted by unique quasi-fiber morphology. The photogenerated electron-hole pair interaction mechanism has been proposed to support the photocatalytic behavior.

1. Introduction

Environmental pollution caused by anthropogenic sources majorly contributes to the overall imbalance of the ecosystem. Release of waste organic dye solution directly into the water system from the textile and small scale industries is a serious problem faced by developed and developing nations in the world. Most of the common pollutants include toxic organic as well as inorganic compounds along with some biological pathogens that are naturally present in the environment. In the recent era, industrial waste water purification using photocatalysis is an active research area of interest [1]. Metal oxide semiconductor photocatalysts offer a way for the treatment of organic contaminants in the presence of solar energy. Visible light-driven oxidation process technology using semiconductor materials has grown for many energy and environmental benefits [2, 3]. The nanostructured ZnO has been studied widely for photocatalytic application [4, 5]. The UV range activity limits the utilization of ZnO as a visible light photocatalyst. Furthermore, the photocatalyst requires further improvement due to its fast recombination rate of the photogenerated electron-hole pairs [6]. Literature reports the augmentation in photocatalytic activity of ZnO by coupling with other semiconductor materials like ZnSe [7], WO_3 [8], CdS [9], and so forth. Among the semiconductors, tungsten oxide semiconductor is worthy of attention due to its small band gap enabling absorption in the visible region, stable physicochemical properties, and resistance to photocorrosion effect [10]. Synthetic attempts to prepare this mixed oxide for photocatalytic purpose are limited in recent literature. Hence, surface modification has been done by loading different amount of WO_3 in ZnO to degrade different dyes [11, 12]. Surface modified ZnO nanorods with WO_3 nanoparticles coated on the surface were synthesized through hydrothermal technique for efficient degradation of endocrine disrupting chemicals like phenol, bisphenol A, and methylparaben under irradiation of 55 W compact fluorescence lamp [12]. In another research, WO_3-ZnO composites were prepared using the wet chemical method and further used to degrade methyl orange. High degradation was observed with 3 mol% WO_3 loaded ZnO under UV light irradiation for 3 h [11]. The existing reports disclose a

maximum 50% efficiency achievement under visible light using WO_3 modified ZnO nanoparticles [13, 14]. The literature lacks in reporting high photocatalytic activity using the visible light after the versatile surface modification. Therefore, the development of WO_3-ZnO nanocomposites is a critical challenge for efficient visible light photocatalytic activity. In the present study, nanocuboid WO_3 and quasi-fibrous ZnO have been prepared by wet chemical methods and assessed the photocatalytic performance of mixed oxide nanocomposites under visible light irradiation. A further comparison has been carried out with reference to commercial ZnO powders with exploration to the charge separation mechanism.

2. Experimental Procedure

2.1. Synthesis of Nanoparticles. Tungsten trioxide (WO_3) nanoparticle was synthesized by hydrothermal treatment of the precipitate solution formed by mixing sodium tungstate dihydrate and 4 M fluoroboric acid at 180°C for 6 hr. The detailed experimental procedure can be found elsewhere [15]. Fluoroboric acid was used as structure directing reagents for the confined growth of WO_3 nanoparticles. The reaction slurry was poured into a Teflon-lined beaker and kept in a hot air oven at prerequisite temperature. The powder obtained was isolated after thorough washing with water and isopropanol followed by drying at 80°C.

In another end, a rapid combustion process was followed to prepare quasi-fibrous ZnO nanoparticles (FZ) at temperature 450°C for 30 min from a gel solution of zinc nitrate hexahydrate and oxalic acid in stoichiometry [16]. Easy dissolution of metal nitrate helps in the formation of the gel. The gel solution was kept in a preheated muffle furnace for combustion. A white porous mass was obtained after the complete reaction.

2.2. Preparation of WO_3-ZnO Nanocomposites. The WO_3-ZnO nanocomposite was prepared by mixing of an optimum amount of 10 wt% WO_3 to 90 wt% ZnO (10% WO_3-FZ) nanopowders using mortar and pestle followed by high-frequency ultrasonication to form a colloidal solution. The colloidal solution was dried at 80°C in the oven with heat treatment at 450°C for 2 hr to establish effective mixing of both the oxides. Similarly, commercial ZnO (CMZ) powder was mixed with nanocuboid WO_3 for the comparative study.

2.3. Characterization of Both Nanoparticles. X-ray diffraction (XRD) patterns for the powders were obtained using a Philips X-ray diffractometer with Ni filtered Cu-Kα radiation (λ = 1.5418 Å). Detailed morphology was studied by transmission electron microscope (JEOL JEM-2100). FESEM and elemental distribution images for both 10 wt% WO_3-FZ and 10 wt% WO_3-CMZ nanocomposites were carried out using Nova NanoSEM FEI-450 system. UV-Visible diffuse reflectance measurement was carried out through Shimadzu spectrophotometer (UV-2450) to evaluate the band gap energy of the individual nanopowders and mixed oxide nanocomposites. Specific surface areas of all the nanopowders were measured using Quantachrome Autosorb, USA, BET apparatus with nitrogen as the adsorbate.

2.4. Photocatalytic Experiments. The photocatalytic experiments were performed in a metal halide reactor containing 50 mL of 20 mg/L aqueous solution of methyl orange (MO) and 50 mg mixed oxide catalyst. The distance between the reactor and the lamp was 2 cm. After each reaction, 2 mL of slurry was taken out and centrifuged for separating the aliquot and catalyst. The UV-Vis absorbance of the aliquot was measured, and catalyst along with the aliquot was poured back to the reaction solution after energetic hand shaking. The degradation efficiency was calculated as follows:

$$\eta = \frac{C_o - C}{C_o} \times 100, \quad (1)$$

where C_o is the absorbance of original MO solution and C is the absorbance of the MO solution after visible light irradiation at certain time interval. The photoactivity of commercial ZnO (CMZ) and nanocomposite of 10 wt% WO_3-CMZ was also carried out for comparison.

3. Results and Discussion

3.1. Phase and Morphological Analysis. XRD pattern is depicted to analyze the phase composition and structure of all WO_3, FZ, CMZ, and 10 wt% WO_3-FZ nanopowders. As shown in Figure 1, all of the peaks of WO_3 are indexed to pure crystalline monoclinic WO_3 (JCPDS Card number 72-0677) crystal phase. The XRD patterns of quasi-fibers ZnO (FZ) and commercial ZnO (CMZ) matches well with the standard hexagonal wurtzite structure (JCPDS Card number 75-0576) where CMZ is found to be highly crystalline in comparison to FZ nanopowders. The 10 wt% WO_3-FZ nanocomposite shows the presence of both monoclinic WO_3 (∗) and hexagonal FZ (#) phases. Figure 2 reveals the FESEM images of all individual nanopowders (WO_3 and ZnO) and 10 wt% WO_3-FZ nanocomposites. Figure 2(a) shows soft agglomerated cuboid-like WO_3 nanoparticles with average length ~142 nm, width ~118 nm, and thickness ~80 nm, respectively. Combustion synthesized ZnO nanopowders have fiber-like morphology which is grown along a confined direction as shown in Figure 2(b). The quasi-fibers are found to have average particle length ~3 μm and width ~0.6 μm, respectively [16]. Commercial ZnO (Figure 2(c)) is represented by highly agglomerated near spherical and anisotropic nanocomposite, whereas cuboid particles are found intimately embedded in the FZ matrix that has been illustrated and confirmed later by FESEM element mapping. The specific BET surface areas of WO_3, FZ, CMZ, and 10% WO_3-FZ are measured to be 5.16 m^2/g, 17.8 m^2/g, 6.19 m^2/g, and 15.9 m^2/g, respectively. A further decrease in surface area to 5.09 m^2/g is observed for nanocomposite prepared using commercial ZnO powders.

In addition, TEM images of WO_3, FZ, and CMZ put forward the clear picture of the nanopowders as represented in Figure 3. The cuboid morphology in Figure 3(a) is found to have average particle length of ~150 nm and width ~120 nm. The tilting of particles at a certain angle shows the imperfect edges of individual cuboids. In FZ (Figure 3(b)), hard agglomeration of spherical particles takes place along one direction to form quasi-fiber-like particles. The in situ particle

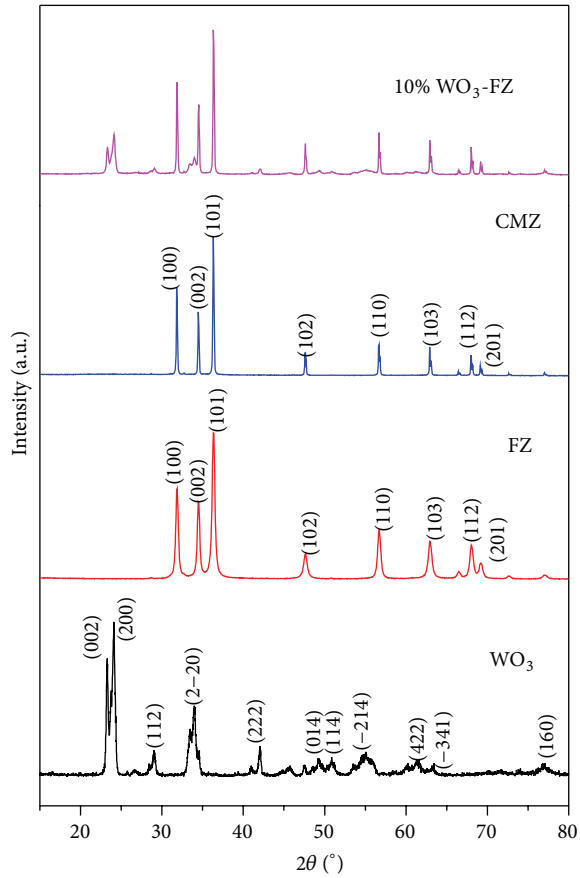

FIGURE 1: Composite X-ray diffraction pattern of WO_3, FZ, CMZ, and 10% WO_3-FZ.

welding takes place along a particular direction during the exothermic reaction forming fibrous structure for ZnO. The spherical particles are found to have average diameter of ~ 55 nm. Different aspect ratio particles are observed for CMZ with average particle size of ~225 nm as shown in Figure 3(c). The particles are seen to have high anisotropy in comparison to synthesized quasi-fiber ZnO.

3.2. Band Gap Determination. Figure 4 shows the UV-DRS spectra pattern of WO_3, FZ, 10% WO_3-FZ, and CMZ, respectively. A distinct right shift of 10% WO_3-FZ nanocomposite (blue color line) has been observed compared to the counterpart pure quasi-fiber ZnO (FZ). This depicts that the optical absorption ability of the nanocomposite persists in the whole range of visible light spectrum [17]. The band gap calculation for the individual nanoparticles and the nanocomposite has been carried out using Tauc plot. The Tauc plot is derived from the square root of Kubelka-Munk function (KMU = $(1-R)^2/2R$, R = reflectance) multiplied by the photon energy and plotted against photon energy ($E_{\text{photon}} = h\nu$). Different degree of band gap energy (E_g) for WO_3, FZ, 10% WO_3-FZ, and CMZ is calculated to be 2.6 eV, 2.95 eV, 3.05 eV, and 3.17 eV, respectively.

3.3. Elemental Analysis of WO_3-ZnO Nanocomposites. Figures 5(a) and 5(b) represent the FESEM elemental mapping of both essential 10% WO_3-FZ and 10% WO_3-CMZ nanocomposites. Individual elements such as W and Zn are represented in green and red color, whereas common blue color homogenously distributed all along the matrix represents the oxygen atom. The distinct morphology clearly demonstrates the intimate contact in between two classes of particles in both the nanocomposites. However, a close look eventually depicts the presence of WO_3 on fibrous ZnO, whereas nanocuboid WO_3 is seen covered by commercial near spherical ZnO particles.

3.4. Photocatalytic Degradation of Methyl Orange. The photocatalytic activity of 10% WO_3-FZ nanocomposite has been studied by degrading methyl orange under metal halide irradiation. As a comparison, degradation of MO with WO_3, ZnO quasi-fibers, commercial ZnO, and 10% WO_3-CMZ photocatalysts is also carried out under similar conditions. Figure 6 shows degradation profile for MO degradation. The degradation graph is plotted with respect to MO concentration as a function of irradiation time C to the initial concentration C_o. It can be seen that only 18% of MO is degraded with individual WO_3 nanopowders. However, a difference of 12% is observed between CMZ and FZ that reveals higher activity of combustion synthesized ZnO than the commercial ZnO photocatalyst. High degradation of 95% is observed in the presence of 10% WO_3-FZ nanocomposites,

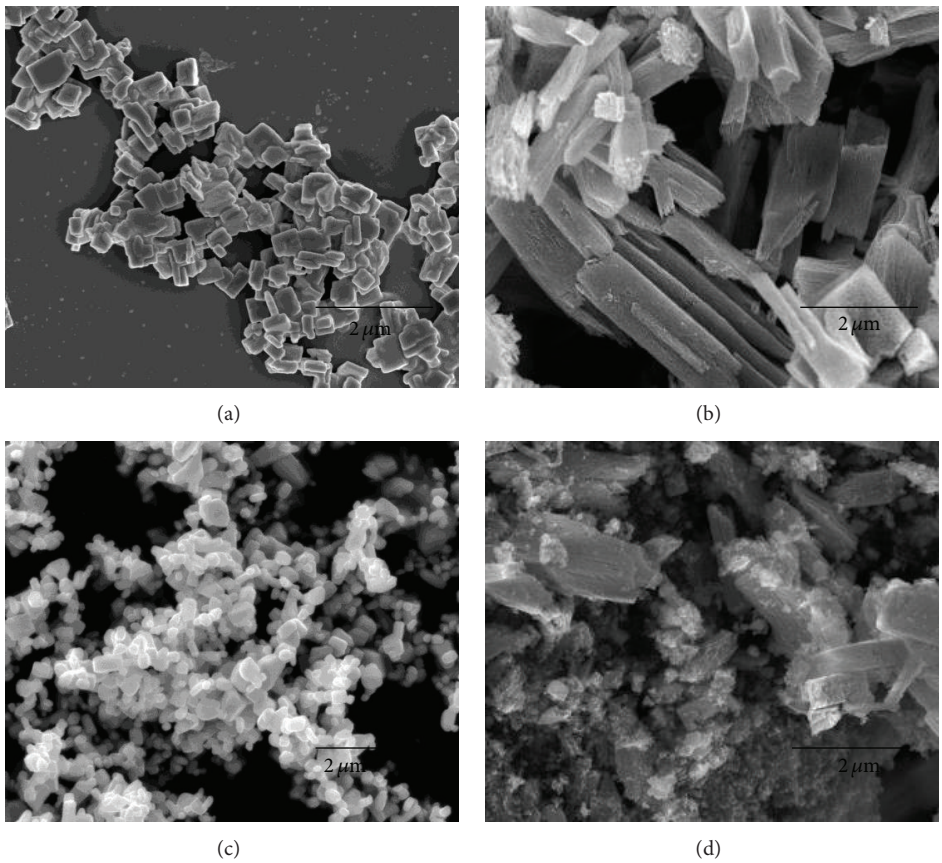

Figure 2: FESEM images of (a) WO_3 nanoparticles, (b) FZ, (c) CMZ, and (d) 10% WO_3-FZ.

whereas a relatively low 85% degradation is observed for 10% WO_3-CMZ.

The degradation kinetics has been calculated following the first-order kinetic equation: $\ln(C/C_o) = -kt$, where k is the first-order rate constant and t is the time [18]. The kinetic constant of FZ is 1.2 times higher than CMZ, whereas the kinetic constant of 10% WO_3-FZ nanocomposite shows 2.0 times higher degradation than 10% WO_3-CMZ, respectively. The correlation coefficient (R^2) observed after linear fitting shows $R^2 > 95$ for all the powders that depicts that the photochemical reaction followed first-order kinetics (Figure 7). Representative photodegradation data of all the powders and nanocomposites is tabulated in Table 1.

Table 1: Representative surface area and photodegradation data of methyl orange.

Sample	Surface area (m^2/g)	% degradation	R^2	k (min^{-1})
WO_3	5.16	18%	0.9679	−0.00221
FZ	17.8	80%	0.9927	−0.01832
CMZ	6.19	68%	0.9531	−0.01277
10% WO_3-FZ	15.9	95%	0.9831	−0.03459
10% WO_3-CMZ	5.09	85%	0.9756	−0.02191

3.5. Photocatalytic Mechanism. The enhanced photocatalytic performance of 10% WO_3-FZ nanocomposite can be attributed to the effective separation of photogenerated electron-hole pairs. However, well elemental dispersion in the WO_3-FZ composite matrix and exposure of large number of active sites due to high surface area of quasi-fibrous ZnO play a vital role in charge separation. Since the composite has a narrow band gap WO_3 and wide band gap ZnO semiconductors, the possible mechanism for the nanocomposite could be harvesting visible light energy through narrow band gap WO_3 present on the surface of quasi-fiber ZnO for excitation of electrons as shown in Figure 8. The recombination of electron-hole pair is reduced via trapping of photoexcited electrons by ZnO to make the system be in equilibrium. These electrons and holes react with surface molecules like O_2 and H_2O to produce superoxide and hydroxyl radical anions. The $^{\bullet}O^{2-}$ and $^{\bullet}OH$ species further reacts with dye molecules to degrade them to lower inorganic molecules like CO_2 and H_2O. Similar observation has been reported for ZnO doped Bi_2O_3 powder under visible irradiation for 6 hr [19].

4. Conclusions

Apparent fusion within primary nanoparticle develops quasi-fiber ZnO during combustion process and structure directing

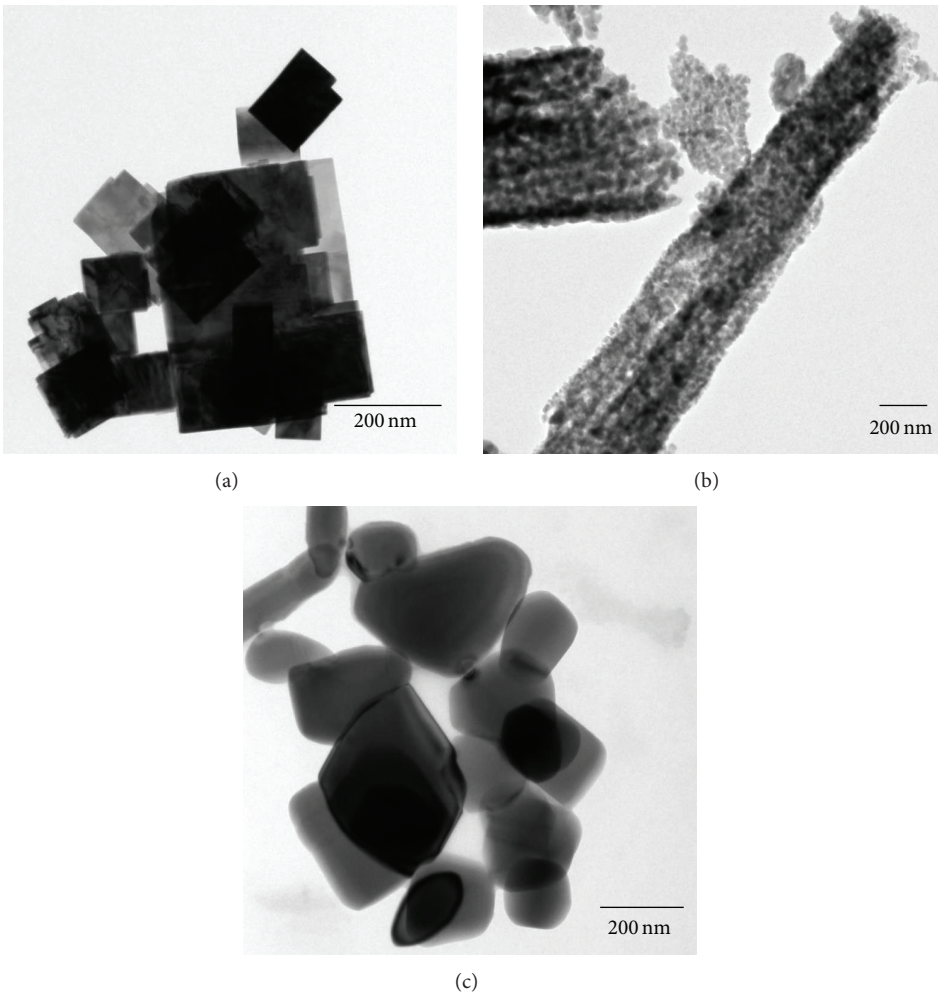

Figure 3: TEM images of (a) WO_3, (b) FZ, and (c) CMZ.

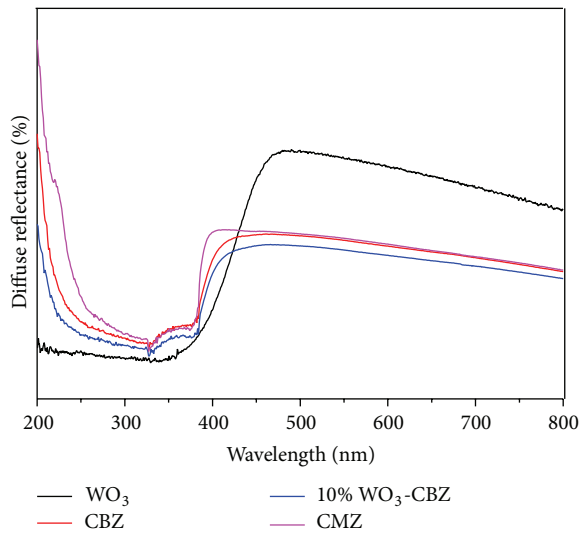

Figure 4: Composite UV diffuse reflectance spectrum.

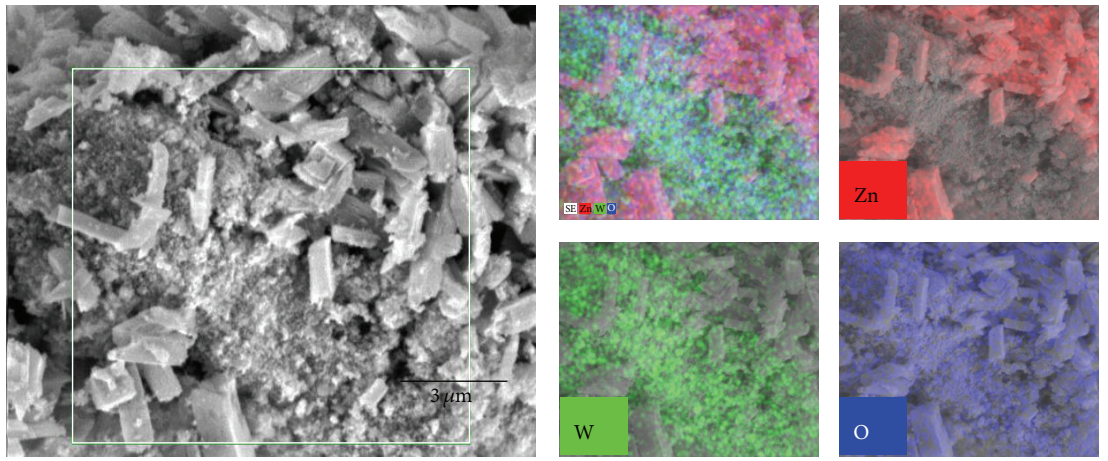

(a)

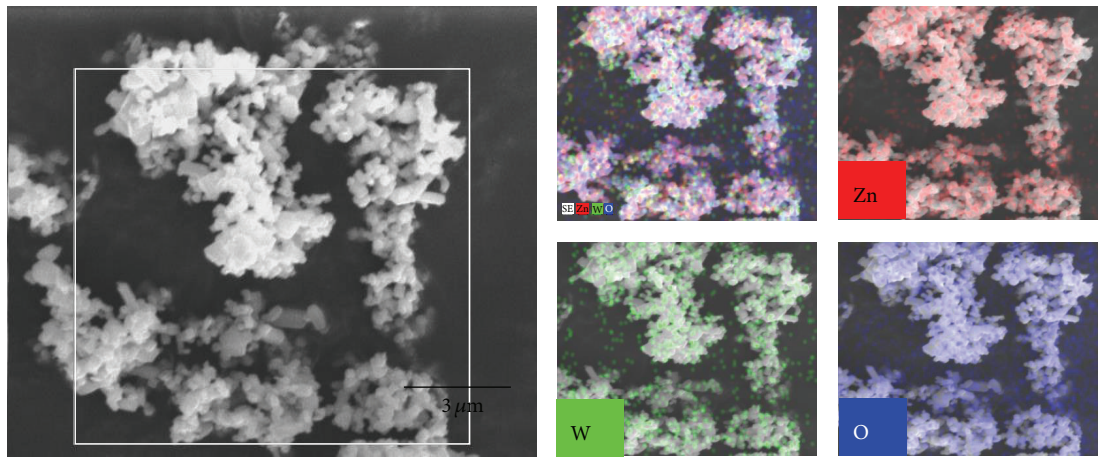

(b)

Figure 5: FESEM elemental mapping of (a) 10% WO_3-FZ and (b) 10% WO_3-CMZ.

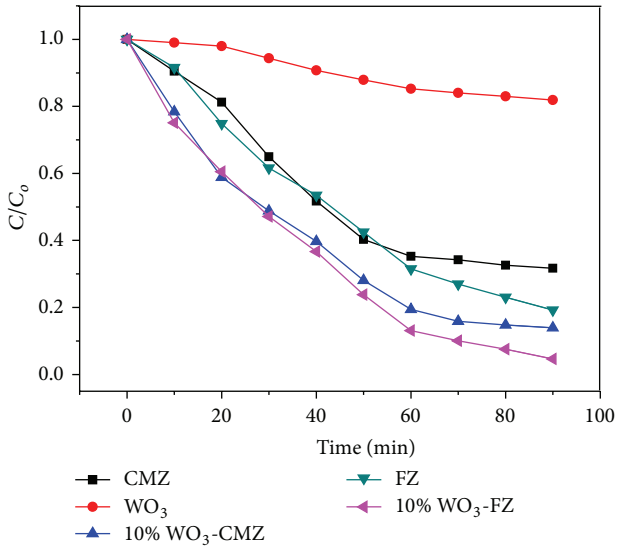

Figure 6: Degradation profile for methyl orange degradation.

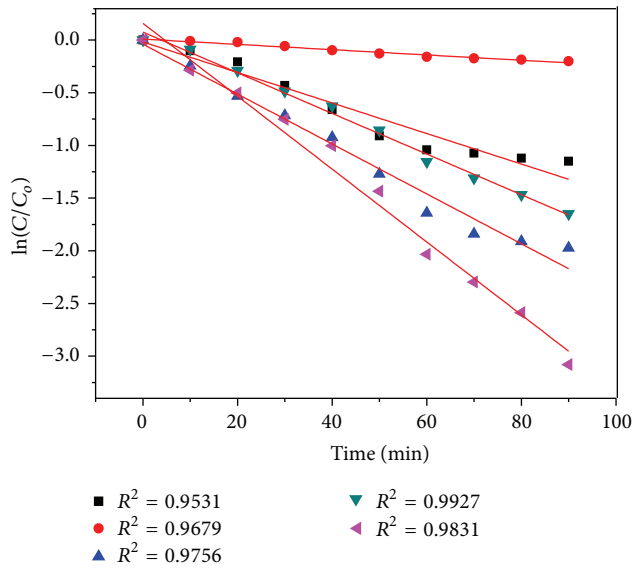

Figure 7: Kinetic profile for methyl orange degradation.

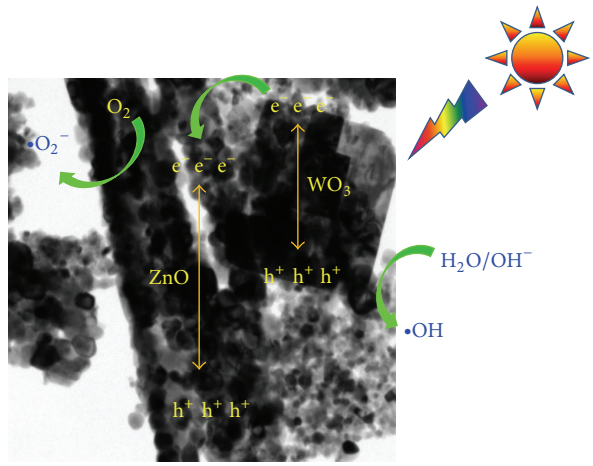

Figure 8: Schematic diagram of WO_3-ZnO photocatalysis.

agent fluoroboric acid directs cuboid shape in WO_3. An optimum amount of 10 wt% nanocuboid WO_3 in quasi-fibrous ZnO matrix is an effective choice for methyl orange dye degradation compared to commercial ZnO nanoparticles. The band gap difference and intimate contact initiate the visible light harvesting and electron excitation and reduce the electron-hole pair recombination to maintain equilibrium in the photochemical system. This process directs the radical reaction and hence subsequent dye degradation. The prepared mixed oxide nanocomposite of WO_3 and ZnO is found as an effective photocatalyst for degradation of organic pollutants in water.

Conflict of Interests

The authors declare that there is no conflict of interests regarding the publication of this paper.

Acknowledgments

The authors would like to thank Department of Science and Technology for research assistance. Special thanks are due to Mr. Subhabrata Chakraborty for FESEM measurements.

References

[1] N. S. Lewis and D. G. Nocera, "Powering the planet: chemical challenges in solar energy utilization," *Proceedings of the National Academy of Sciences of the United States of America*, vol. 103, no. 43, pp. 15729–15735, 2006.

[2] K. Maeda, T. Takata, M. Hara et al., "GaN:ZnO solid solution as a photocatalyst for visible-light-driven overall water splitting," *Journal of the American Chemical Society*, vol. 127, no. 23, pp. 8286–8287, 2005.

[3] R. Asahi, T. Morikawa, T. Ohwaki, K. Aoki, and Y. Taga, "Visible-light photocatalysis in nitrogen-doped titanium oxides," *Science*, vol. 293, no. 5528, pp. 269–271, 2001.

[4] G. Wang, D. Chen, H. Zhang, J. Z. Zhang, and J. H. Li, "Tunable photocurrent spectrum in well-oriented zinc oxide nanorod arrays with enhanced photocatalytic activity," *The Journal of Physical Chemistry C*, vol. 112, no. 24, pp. 8850–8855, 2008.

[5] J. Bae, J. B. Han, X.-M. Zhang et al., "ZnO nanotubes grown at low temperature using ga as catalysts and their enhanced photocatalytic activities," *Journal of Physical Chemistry C*, vol. 113, no. 24, pp. 10379–10383, 2009.

[6] L. R. Zheng, Y. H. Zheng, C. Q. Chen et al., "Network structured SnO_2/ZnO heterojunction nanocatalyst with high photocatalytic activity," *Inorganic Chemistry*, vol. 48, no. 5, pp. 1819–1825, 2009.

[7] W. Chen, N. Zhang, M. Y. Zhang, X. T. Zhang, H. Gao, and J. Wen, "Controllable growth of ZnO-ZnSe heterostructures for visible-light photocatalysis," *CrystEngComm*, vol. 16, no. 6, pp. 1201–1206, 2014.

[8] B. Subash, B. Krishnakumar, B. Sreedhar, M. Swaminathan, and M. Shanthi, "Highly active WO_3-Ag-ZnO photocatalyst driven by day light illumination," *Superlattices and Microstructures*, vol. 54, no. 1, pp. 155–171, 2013.

[9] J. Nayak, S. N. Sahu, J. Kasuya, and S. Nozaki, "CdS–ZnO composite nanorods: synthesis, characterization and application for photocatalytic degradation of 3,4-dihydroxy benzoic acid," *Applied Surface Science*, vol. 254, no. 22, pp. 7215–7218, 2008.

[10] H. Zheng, J. Z. Ou, M. S. Strano, R. B. Kaner, A. Mitchell, and K. Kalantar-Zadeh, "Nanostructured tungsten oxide—properties, synthesis, and applications," *Advanced Functional Materials*, vol. 21, no. 12, pp. 2175–2196, 2011.

[11] J. Xie, Z. Zhou, Y. Lian et al., "Simple preparation of WO_3-ZnO composites with UV-Vis photocatalytic activity and energy storage ability," *Ceramics International*, vol. 40, no. 8, pp. 12519–12524, 2014.

[12] S.-M. Lam, J.-C. Sin, A. Z. Abdullah, and A. R. Mohamed, "ZnO nanorods surface-decorated by WO_3 nanoparticles for photocatalytic degradation of endocrine disruptors under a compact fluorescent lamp," *Ceramics International*, vol. 39, no. 3, pp. 2343–2352, 2013.

[13] C. Yu, K. Yang, Q. Shu, J. C. Yu, F. Cao, and X. Li, "Preparation of WO_3/ZnO composite photocatalyst and its photocatalytic performance," *Chinese Journal of Catalysis*, vol. 32, no. 3-4, pp. 555–565, 2011.

[14] Y. Wang, L. Cai, Y. Li, Y. Tang, and C. Xie, "Structural and photoelectrocatalytic characteristic of ZnO/$ZnWO_4$/WO3 nanocomposites with double heterojunctions," *Physica E: Low-Dimensional Systems and Nanostructures*, vol. 43, no. 1, pp. 503–509, 2010.

[15] S. Adhikari and D. Sarkar, "Hydrothermal synthesis and electrochromism of WO_3 nanocuboids," *RSC Advances*, vol. 4, no. 39, pp. 20145–20153, 2014.

[16] S. Adhikari, D. Sarkar, and G. Madras, "Synthesis and photocatalytic performance of quasi-fibrous ZnO," *RSC Advances*, vol. 4, no. 99, pp. 55807–55814, 2014.

[17] S. Wei, Z. Shao, X. Lu, Y. Liu, L. Cao, and Y. He, "Photocatalytic degradation of methyl orange over ITO/CdS/ZnO interface composite films," *Journal of Environmental Sciences*, vol. 21, no. 7, pp. 991–996, 2009.

[18] J. Matos, J. Laine, and J. M. Hermann, "Synergy effect in the photocatalytic degradation of phenol on a suspended mixture of titania and activated carbon," *Applied Catalysis B: Environmental*, vol. 18, no. 3-4, pp. 281–291, 1998.

[19] C. Chen, J. Weng, J. Chen et al., "Photocatalyst ZnO-doped Bi_2O_3 powder prepared by spray pyrolysis," *Powder Technology*, vol. 272, pp. 316–321, 2015.